Temporal order of signal propagation within and across intrinsic brain networks

Mike J. Veit[a], Aaron Kucyi[b], Wenhan Hu[c,d], Chao Zhang[c], Baotian Zhao[c], Zhihao Guo[c], Bowen Yang[c], Clara Sava-Segal[a], Claire Perry[a], Jianguo Zhang[c,d], Kai Zhang[c,d,1], and Josef Parvizi[a,1]

[a]Department of Neurology & Neurological Sciences, Stanford University, Stanford, CA 94305; [b]Department of Psychology, Northeastern University, Boston, MA 02115; [c]Department of Neurosurgery, Beijing Tiantan Hospital, Capital Medical University, Beijing 100070, China; and [d]Stereotactic and Functional Neurosurgery Laboratory, Beijing Neurosurgical Institute, Capital Medical University, Beijing 100070, China

Edited by Marcus E. Raichle, Washington University in St. Louis, St. Louis, MO, and approved October 27, 2021 (received for review March 24, 2021)

We studied the temporal dynamics of activity within and across functional MRI (fMRI)–derived nodes of intrinsic resting-state networks of the human brain using intracranial electroencephalography (iEEG) and repeated single-pulse electrical stimulation (SPES) in neurosurgical subjects implanted with intracranial electrodes. We stimulated and recorded from 2,133 and 2,372 sites, respectively, in 29 subjects. We found that N1 and N2 segments of the evoked responses are associated with intra- and internetwork communications, respectively. In a separate cognitive experiment, evoked electrophysiological responses to visual target stimuli occurred with less temporal separation across pairs of electrodes that were located within the same fMRI-defined resting-state networks compared with those located across different resting-state networks. Our results suggest intranetwork prior to internetwork information processing at the subsecond timescale.

CCEP | event related potentials | intracranial EEG | gradual-onset continuous performance task | human

It has been known for a while that certain regions of the brain have correlated activity, forming "intrinsic networks" that can be identified while people are resting (*SI Appendix*, Table S1). These correlated activities were first discovered by measuring blood-oxygenation level–dependent (BOLD) signals and later confirmed with measures of electrophysiological activity (1–10). In a series of studies, we and others have shown that distinct sites of the cerebral cortex that are part of a functional MRI (fMRI)–defined intrinsic network become coactivated during an experimental task and are connected at rest via slow fluctuations of their local high-frequency broadband (HFB) power (5–10).

Much of what we know about the resting-state intrinsic networks has been gleaned from studies that have relied on neural data within a slow temporal domain. As a result, the temporal dynamics of activity within and across these intrinsic networks remain almost entirely unknown. Such information may provide core mechanistic information about the functional architectural design of our brains.

To address this unknown, we collected information from a relatively large number of recording sites in a group of human subjects implanted with intracranial electrodes as part of their clinical diagnostic workup. In each subject, repeated single electrical pulses were delivered intracranially in specific electrode sites while we recorded evoked responses from hundreds of other intracranial electrodes as routinely performed in clinical centers (11). This method, known as single-pulse electrical stimulation or corticocortical evoked potential (CCEP), allows one to explore the presence or absence of signal flow and its timing between a stimulated region and hundreds of target areas (i.e., those implanted with recording electrodes). The high temporal resolution of this method combined with precise anatomical information about the sites of stimulation and recording allows for measurements down to the millisecond timescale and millimeter precision (12). Also, because the source of the signal and time of evoked responses are known, this method provides indirect information about possible directionality of the propagation of electrophysiological signals within the brain. The prevailing current hypothesis is that direct anatomical connectivity between the seed and target regions will evoke sharper and faster responses while second-order connections are thought to evoke slower and dispersed responses (13, 14).

Results

Single electrical pulses were delivered individually to 2,133 cortical sites and recorded in 2,372 sites across 29 subjects (Fig. 1 and *SI Appendix*, Fig. S1 and Table S2). Our final sample therefore yielded 33,721 unique paired time series across all subjects. Since stimulations and recordings were performed in a bipolar manner (i.e., between two adjacent electrodes), each time series corresponded to one pair of electrodes that was stimulated and one pair that was recorded from.

In keeping with the large body of CCEP literature, we found that the morphology of the evoked responses was highly heterogeneous across electrode pairs. While some had an early sharp peak (usually termed the N1 peak, 10 to 50 ms), other responses were late and less sharply contoured (slow wave-like potential often termed the N2 peak, 50 to 200 ms). Some showed large N1 and N2 peaks while others showed only an N2 peak. This heterogeneity of the number and latency of observed peaks in a CCEP response has been well-documented (13, 15).

Next, we extended our previous findings (16) to the whole-brain level and tested the hypothesis that the timing of evoked responses would depend on the network identity of the seed and target areas being evaluated. For this, we first used a

Significance

Direct electrical stimulation and intracranial recordings from the human brain during cognitive experiments revealed unique information about the temporal order of signal processing within and across intrinsic resting-state networks. Pairs of regions located within the same intrinsic networks communicate faster and coactivate closer in time than those located across different intrinsic networks.

Author contributions: M.J.V. and J.P. designed research; M.J.V., A.K., W.H., C.Z., B.Z., Z.G., B.Y., C.S.-S., and C.P. performed research; A.K., W.H., C.Z., B.Z., Z.G., B.Y., J.Z., K.Z., and J.P. contributed new reagents/analytic tools; J.Z., K.Z., and J.P. supported with funding; M.J.V. and A.K. analyzed data; and M.J.V., A.K., and J.P. wrote the paper.

The authors declare no competing interest.

This article is a PNAS Direct Submission.

[1]To whom correspondence may be addressed. Email: zhangkai62035@sina.com or jparvizi@stanford.edu.

This article contains supporting information online at http://www.pnas.org/lookup/suppl/doi:10.1073/pnas.2105031118/-/DCSupplemental.

Published November 24, 2021.

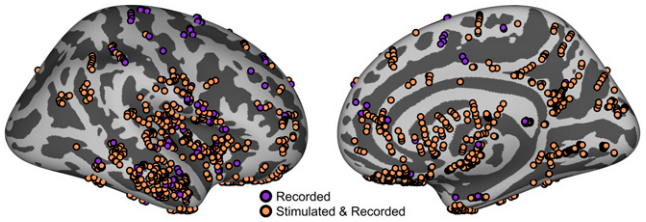

Fig. 1. Distribution of implanted electrodes. Signal from each electrode was continuously recorded during stimulation and task performance. Purple electrodes (n = 239) were recorded but not stimulated. Orange electrodes (n = 2,372) are those that were recorded from and also used as seeds for stimulations. Electrodes cover all lobes and all intrinsic cortical networks.

k-means clustering algorithm to characterize the distribution profile of the time to first peak according to the network identity of each time series. We found three clusters of electrodes (Fig. 2*A*; cluster 1: 0 to 55 ms; cluster 2: 55 to 107 ms; cluster 3: 107 to 200 ms). The average response for each of the three clusters is shown in Fig. 2*B*. Responses in the fastest cluster showed a sharp N1 peak with a following broad N2 peak, while the slower two clusters showed only an N2 peak without an N1 peak. We then used a permutation test to determine the network signatures of each of the three identified clusters. As shown in Fig. 2*C*, two clear dissociated patterns were identified. Most importantly, we discovered that the fastest responses with N1 peaks (cluster 1) were predominantly intranetwork responses (i.e., the stimulated and recorded electrodes belonged to the same intrinsic network). The fastest cluster contained all possible intranetwork connections except the frontoparietal intranetwork connection, which is not present in any of the three clusters. This is likely due to the low number of these intranetwork responses in our dataset lowering the sensitivity for this intranetwork connection (*SI Appendix*, Fig. S2). By contrast, the slower two clusters with only N2 peaks (clusters 2 and 3) contained exclusively internetwork responses.

In addition to intranetwork signals occurring only in the fastest cluster, the slower two clusters shed light on the directionality of the speed of propagation between certain networks. For example, the default-to-visual signals are in the middle cluster (cluster 2) whereas the visual-to-default signals are in the slowest cluster (cluster 3). This implies that the speed of signal propagation is not homogeneous between networks and also depends on the direction of the propagation. However, we are mindful that the directionality of signal propagation across networks as we report here needs to be explored and validated further across a large sample of subjects with near-identical pairs of stimulation and recording sites across given networks of interest.

To ensure that the CCEP findings were not sensitive to the choice of the number of clusters, we repeated the analysis for two to seven clusters (*SI Appendix*, Fig. S3). In all of these

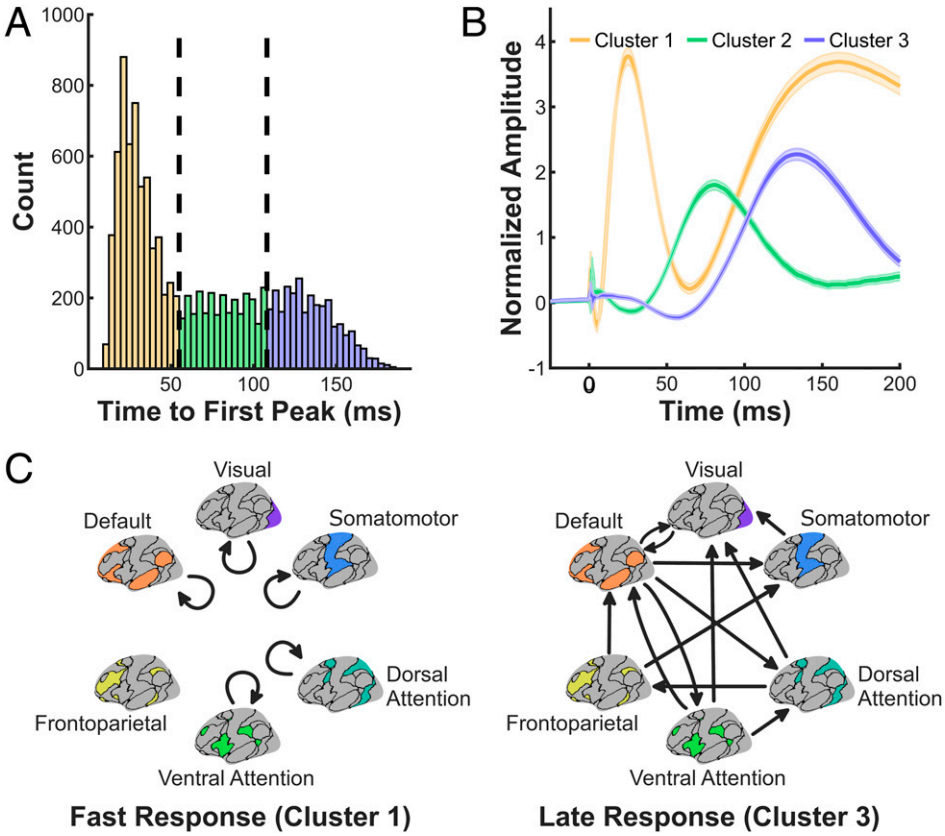

Fig. 2. Temporal signature of intra- and internetwork signal flow. (*A*) Histogram of the time to first peak for the time series of each stimulation–record electrode pair. Colors indicate the three clusters generated from a k-means algorithm with borders at 55 and 107 ms (dashed lines). (*B*) Average normalized evoked potentials for the three clusters shown in *A*. The morphology of the average responses shows that cluster 1 contains evoked responses which have an N1 and N2 peak while clusters 2 and 3 only contain N2 peaks. (*C*) Network signatures for the fast responses (cluster 1) and the late responses (cluster 3) generated by permutation analysis. It is clear that the fast response is dominated by intranetwork connections while the late response contains most of the internetwork connections. Cluster 2 also exclusively showed four internetwork responses, and the detailed network connections can be found in *SI Appendix*, Table S3. Note this analysis generates the most prevalent connections. Therefore, if a connection is not shown it does not mean that it does not exist at all, but it is not a major component of the cluster.

analyses, the intranetwork responses are dominant in the fastest clusters. Therefore, our major result that intranetwork signals propagate faster on average than internetwork signals is not dependent on the number of clusters. Furthermore, a plot of the sum of squared errors versus the number of clusters shows a sharp kink at $k = 3$, suggesting that three clusters is the optimal choice.

We also reexamined our results to explore whether a shorter Euclidean distance between intranetwork compared with internetwork pairs could explain our findings. The average distance between intranetwork pairs was 49.5 mm (SD 24.1 mm, n = 25,430) and between internetwork pairs was 44.8 mm (SD 23.1 mm, n = 8,291). Therefore, both internetwork and intranetwork time series measured long-distance responses, and Euclidean distance alone cannot explain our results.

To validate the result that intranetwork signals generally propagate faster than internetwork signals, we conducted a parallel study to analyze the timing of task-evoked electrophysiological responses. For this, we asked the same participants to perform a gradual-onset continuous performance task (gradCPT; Fig. 3*A*) (17, 18).

We recorded induced HFB (70- to 170-Hz) neural responses to behaviorally relevant stimuli. We chose this experimental task because it engages all six intrinsic networks (visual stimuli, subject responses by mouse click, top-down sustained attention, and bottom-up attention as well as withdrawal of habitual responses to infrequent oddball stimuli). We have shown previously that this task leads to negative deflections in HFB power amplitude in the default network and positive deflections in HFB power amplitude in several networks such as visual, ventral attention, dorsal attention, and frontoparietal executive networks (18–20). We hypothesized that two regions will show HFB responses closer in time if the two sites are in the same fMRI-defined intrinsic network. Indeed, this was the case. Probability distributions of the absolute difference in time to peak for intra- and internetwork pairs confirmed a clear difference in the distributions and a 44-ms difference in median times ($P < 0.0001$ by the two-sided Wilcoxon rank-sum test) with intranetwork signals appearing closer in time on average than internetwork signals (Fig. 3*B*). A mixed-effect model was also implemented to adjust for the hierarchical nature of the data with multiple responses measured from a single patient and the distance dependence of the time to peak difference (*SI Appendix*, Fig. S4). This model produced a coefficient of a 67.6-ms (95% CI: 100.0 to 35.2 ms; $P < 0.0001$) difference between inter- and intranetwork responses (*SI Appendix*, Table S4), indicating that neither had a significant effect on the results.

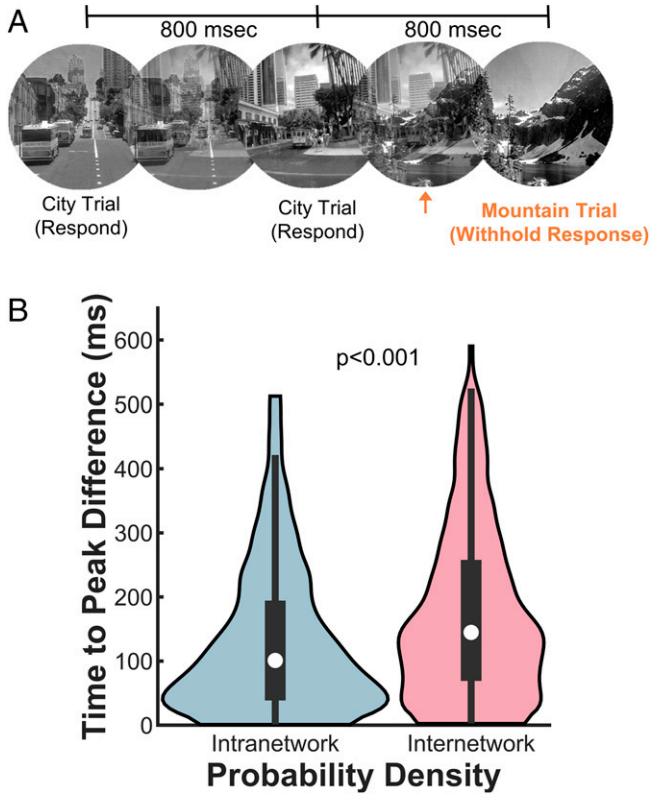

Fig. 3. Experimental data. (*A*) Design for the gradCPT task illustrating the gradual transition between images which leads to the activity seen by iEEG. Grayscale visual images of either city or mountain scenes gradually transitioned from one to another every 800 ms. The subject is instructed to press a button when a city appears but to withhold response when a mountain is noticed. (*B*) Probability distributions for the difference in time to peak of regional HFB activity during the experiment for pairs of electrodes within (n = 274) or across (n = 478) networks. The distributions are highly dissimilar. Intranetwork electrode HFB activity is significantly closer in time than the HFB activity in pairs of electrodes located across different networks. The median time difference is 44 ms faster in intranetwork electrodes, and this difference is statistically significant at the $P < 0.001$ level.

Discussion

We used two independent methods and confirmed that signal flow within the human brain follows a temporal order: Early processing of signals within the same functional networks is followed by later cross-network communications. In the context of recent results which combined CCEP and diffusion-weighted imaging (21), it is likely that this faster intranetwork propagation is a measurement of a preferential structural connectivity within the networks. While the data presented here cannot provide a definitive statement on such connections, it adds to a growing body of evidence that fMRI resting-state networks partially reflect the underlying structure of the human brain (22).

The strength of our findings is remarkable especially given the limitations of our methodology. For instance, we relied on a coarse segregation of the human brain into six intrinsic networks defined in the standard reference brain space. In reality, we may be dealing with a much higher number of networks than six. More importantly, the "network membership" of the electrodes was determined only by transferring the location of electrodes from a native anatomical space to the standard space (23). By doing so, we caused a shift in the location of electrodes depending on the differences between the native and standard brain spaces. Although we attempted to minimize this by conservatively using only areas of the atlas that have a high confidence in network assignment, we are mindful that a transfer from native space to standard space could lead to missing the effects of subject-specific anatomy and network distribution. Utilizing native anatomical space information with individual-level fMRI was unfortunately not feasible in our current study. Such recordings in the future may provide a more fine-grained map of signal exchanges using individual brain space fMRI data.

The second limitation of our measures pertains to the use of gradCPT task design which makes the HFB onset of a given trial variable given that the stimuli are gradually fusing with each other. This causes more variability in the time to peak used in our analysis. While this potential bias is nondifferential between intra- and internetwork pairs, it produces significant variance in the measured times to HFB peaks and may make the measurement less precise. However, we have previously found that the HFB response onsets to gradual-onset target stimuli within default, dorsal attention, and salience network regions (18) are comparable to those found in tasks involving more abrupt stimulus onsets (8, 24). It will be important to

further validate and extend our findings using distinct task paradigms involving a wider range of stimuli.

We and others (15, 25, 26) have shown that epilepsy significantly alters the speed of signal flow in the human brain which in turn could have affected our results. Epileptic electrode sites in our cohort, which were clinically determined, constituted only a very low percentage of the total contacts in our entire dataset. Of the 33,721 CCEP time series used in the analysis, only 525 either stimulated or recorded from an electrode contact that was determined to be in the seizure-onset zone. We reran our analysis by excluding these contacts and found the results to be identical to the original analysis. Similarly, none of the task-evoked responses used in our analysis involved a contact which showed spontaneous epileptic activity. Additionally, none of the patients experienced a seizure during either the CCEP or task-based measurements. We therefore believe that recording from or stimulating epileptic regions of individual patients was not a significant confounder. We cannot definitively exclude the possibility that the connectivity of other regions may be affected by the epileptic activity. However, such individual-specific changes likely averaged out over the large number of patients in our dataset.

In conclusion, our study provides a map of the timing of signal flow within and across networks in the human cortex with high temporal resolution. Convergence of findings across two separate methods gives us confidence that our findings are not an artifact of our measurements. Our mapping covers intrinsic networks across the human brain (though at a coarse level) and provides a greater understanding of how physiological signals are processed at the millisecond level.

Methods

Subject Details. Twenty-nine subjects (mean 26 y of age; 43% male) with focal epilepsy were recruited in this study. Each subject underwent implantation of depth intracranial electrodes at Beijing Tiantan Hospital to localize their seizures, with the location of electrodes determined solely by clinical needs. Depth electrode contacts (HKHS Healthcare) had a contact length of 2 mm, diameter of 0.8 mm, and interelectrode spacing of 1.5 mm. All participants gave written informed consent before their participation. This study was approved by the Medical Ethics Committee of Beijing Tiantan Hospital.

Electrical Stimulation. Single-pulse stimulations were performed with a bipolar setup using a cortical stimulator while the subjects were awake and resting. Single pulses of electrical current (5 mA, biphasic, 500 μs per phase) were injected between pairs of adjacent intracranial electrodes at a frequency of 0.5 Hz. Data were recorded with a Nihon Kohden system using a sampling rate of 1,000 Hz. The recording system included a band-pass filter of 0.08 to 300 Hz to exclude slow varying and high-frequency effects. The number of stimulation trials varied between subjects and electrode pairs due to time constraints (range 3 to 80; mean 39). Electrical potentials were simultaneously measured in all other electrodes with a sampling rate of 1,000 Hz.

Discarded Data. As we were interested in only the cortical networks, electrodes in the white matter and subcortex were excluded. Specifically, we kept only electrodes which contained at least 1 gray matter voxel within a 2-mm sphere centered on the electrode. To minimize volume conduction effects, we also discarded data recorded from electrodes on the same electrode shaft as the stimulated electrode.

Analysis of Evoked Responses. Electrode signals were first rereferenced to a bipolar montage. Evoked responses in nonstimulated electrodes were then segmented into 225-ms epochs (25 ms prestimulus and 200 ms poststimulus) which were time-locked to the delivery of the stimulus. Time series data were normalized to the mean and SD of the first 20 ms of the epoch (i.e., −25 to −5 ms) and averaged over all trials of a given stimulation. Because the direction of activity is ambiguous in data collected from bipolar electrodes, we chose the sign of the time series so that the maximum evoked response was positive (13). Finally, peaks were detected using MATLAB's peak detection algorithm and a minimum prominence was set as seven times the SD of the mean prestimulus baseline for each time series. All time series which did not show a significant response were discarded from the analysis.

Neuroimaging Acquisition. In a preoperative MRI session, all subjects underwent structural MRI (T1-weighted). In addition, a computed tomography (CT) scan was obtained following electrode implantation, which was used for anatomical localization of electrode contacts. Neuroimaging was performed at Beijing Dongzhimen Hospital on a 3.0-T Siemens MAGNETOM Verio System with a 32-channel head coil. For T1 scans, an MPRAGE sequence was acquired with parameters 256 × 256 matrix, 176 slices, 1.00 × 1.00 × 1.00–mm voxels, 9° flip angle, 1,900-ms repetition time, and 2.53-ms echo time.

Anatomical Localization of Electrode Contacts. We used the iELVis pipeline (27) for anatomical localization of electrode contacts. First, we processed and reconstructed the T1 scan using FreeSurfer v6.0.0 (recon-all command) (25). We then aligned the postimplant CT image to the preimplant T1 scan using a rigid transformation (six-degree-of-freedom affine mapping). Using BioImage Suite (28), we manually labeled each electrode location on the T1-registered CT image. The electrode coordinates obtained from this approach were used for visualization and to assign electrodes to networks of interest.

Network Membership Assignment. Electrodes were assigned to the nearest Yeo 7 networks (23) as determined by the iELVis parcellation algorithm after mapping the patient-specific electrode locations to the standard Yeo 7 atlas. Furthermore, because of the limbic network's functional and anatomical proximity to the default network (29) and because the limbic network is often in the signal dropout zone of fMRI leading to low confidence in network assignment, electrodes assigned to the limbic network by this algorithm were instead assigned to the default network. We took two additional steps to ensure this network assignment was as accurate as possible to the true network despite the lack of subject-specific fMRI data. First, if electrodes in a pair of the bipolar montage (i.e., immediate neighbors) were assigned different networks using this method, we discarded the pair from further analysis. This ensured that we were not stimulating multiple networks or recording from multiple networks. Second, the confidence of the network assignment in the Yeo 7 atlas is not uniform across the entire brain (23). In particular, the boundaries between networks have low confidences. We therefore set a threshold confidence (threshold 0.3), and all electrodes below that threshold were discarded from further analysis.

Clustering Analysis. The time to the first peak in the evoked response for each time series (mean across trials) was used as the figure of merit for connectivity between the stimulated electrodes and the recorded electrodes. There were two benefits of this compared with using the strength of the signal. First, there was only a very weak dependence from the Euclidian distance between the pairs of electrodes (*SI Appendix*, Fig. S5) whereas the strength of the signal is strongly dependent on the distance. This therefore minimizes the effects of distance between electrodes. Second, this method detects the presence of an N1 peak. The time to first peak therefore is a measure of the directional connectivity between the two regions. The time to peak was concatenated across all mean time series from all subjects and then clustered using a *k*-means algorithm using the squared time difference as the distance metric to find two to seven clusters.

Permutation Testing. To determine the network signature of each cluster, we used a hierarchical bootstrap method. We compared the frequency of each pair of networks with a null distribution generated by permutations. The directionality of signal propagation was maintained when calculating the frequencies, so a different frequency was calculated for stimulating network A and measuring network B from the frequency calculated for stimulating network B and measuring network A. The permutations were generated at the subject level and then combined at the group level to account for the hierarchy of the data at the subject level. The network identities of all the time series were shuffled and the frequency of every directed network pair was calculated for each cluster. This was repeated for 100,000 permutations. Network connection pair frequencies for the true network assignments which were more extreme than the highest 0.5% from the permutation frequency distribution were taken to be significant. This approach identifies the directional connections among the networks in each cluster for which we could reject the null hypothesis.

GradCPT Task. Out of the 29 subjects who underwent CCEP procedures, 18 subjects additionally performed the gradCPT (17), administered in three to seven runs, each lasting 6 or 8 min, as described previously (18). The task was administered at bedside via a laptop running Windows 8.1. Stimuli were presented using Psychophysics Toolbox in Matlab R2016b (MathWorks). Transistor–transistor logic pulses were sent to an empty channel on the electroencephalography (EEG) montage to mark the onset times of each stimulus.

In the gradCPT, grayscale visual images of either city or mountain scenes gradually transitioned from one to another for the duration of the task. Each transition lasted 800 ms, with image coherence gradually increasing at the trial onset and then decreasing toward the trial end. Scene categories were presented randomly at a rate of either 10 mountain and 90% city or 25 mountain and 75% city (10 unique images, respectively, for each category). The order of these images was randomized during each run. Participants were instructed to press the space bar on the laptop when they noticed a city appearing but to withhold response when they noticed a mountain appearing. Participants performed with their dominant hand, except in situations where there was discomfort of the dominant hand.

GradCPT Intracranial EEG Data Preprocessing. The gradCPT intracranial EEG (iEEG) data were preprocessed with a previously established pipeline (20). Notch filtering was performed to attenuate powerline noise at 50 Hz and its harmonics (zero-phase, third-order, Butterworth filter with a band stop between 47 and 53, 97 and 103, and 147 and 153 Hz). Signals were then rereferenced from each channel to the common average signal across all channels, with the channels excluded from the common average if they met one of the following criteria: 1) showed pathological activity during clinical monitoring (as noted by a neurologist); 2) were manually labeled as outliers based on visual inspection of power spectra; 3) had a variance greater or lesser than five times the median variance across all channels; or 4) had greater than three times the median number of spikes across all channels, with spikes defined as 100-μV changes between successive samples. We performed time–frequency decomposition using a Morlet wavelet transform with frequency bands log-spaced between 1 and 170 Hz (38 total values). For each frequency band, we rescaled each time sample by the log ratio of the whole run's power amplitude time series (i.e., to account for band-specific 1/*f* decline of the power spectrum). Subsequently, power amplitude was averaged within the HFB (70- to 170-Hz) range, and minimal temporal smoothing was applied with a 50-ms Gaussian kernel.

Time-to-Peak Analysis of Task-Evoked HFB Responses. We computed the time to peak (TTP) of HFB responses to mountain (target) trials in the gradCPT for electrodes that were defined as "task-responsive." This analysis was limited to electrodes that were included in the CCEP analyses. Task-responsive channels were defined based on mountain (i.e., target)-evoked HFB responses during correct omission trials (withholding a button press when a target stimulus appears) (20). This was based on a decreased target-evoked HFB response for default-mode network (DMN) sites and an increased target-evoked response for non-DMN sites. To define task-responsive electrodes, we used a nonparametric cluster-based permutation test (30) to compare HFB power amplitude during target relative to baseline trials (combining trials across all task runs within each participant). The cluster-based permutation test was based on the time window of 0 to +1,500 ms relative to trial onset (i.e., beginning of stimulus fading in). An electrode was considered task-responsive if it showed a significant temporal cluster at the level of Monte Carlo one-tailed (decrease for DMN, increase for non-DMN) $P < 0.001$ (uncorrected for multiple comparisons). For all electrode pairs that were included in the CCEP analysis, we identified those in which both electrodes were task-responsive. For each of those pairs, we computed TTP as the minimum (DMN electrodes) or maximum (non-DMN electrodes) peak time point of HFB power amplitude (averaged across trials) within a time window ranging from +200 to +1,500 ms after trial onset (18).

We then computed the absolute TTP difference for each electrode pair. The electrode pairs were then grouped into internetwork and intranetwork pairs. The resulting internetwork and intranetwork TTP probability distributions were compared using the two-sided Wilcoxon rank-sum test. This tests the null hypothesis that the two samples come from distributions with equal medians against the alternative hypothesis that they are not. In order to adjust for the hierarchical nature of the data, we also implemented a linear mixed-effect model adjusting for distance between contacts and whether the contacts were within the same network and allowed for an independent random slope and intercept at the patient level. This model included fixed effects for distance between contacts and whether the contacts were within the same network as well as uncorrelated random effects for intercept, distance, and intranetwork status grouped by the patient ID.

Data Availability. The entire dataset used in this publication has been deposited in FigShare (https://figshare.com/projects/Temporal_Order_of_Signal_Propagation_Within_and_Across_Intrinsic_Brain_Networks/123283).

ACKNOWLEDGMENTS. We thank members of the Tiantan team for assistance with data collection. This work was supported by NIH research grant 1R21NS113024 (to J.P.); National Natural Science Foundation of China (Grants 81771399 and 81701276 to K.Z.); China Scholarship Council (Grant 201908110041 to C.Z.); and Banting Fellowship from the Canadian Institutes of Health Research (to A.K.).

1. B. Biswal, F. Z. Yetkin, V. M. Haughton, J. S. Hyde, Functional connectivity in the motor cortex of resting human brain using echo-planar MRI. *Magn. Reson. Med.* **34**, 537–541 (1995).
2. G. L. Shulman *et al.*, Common blood flow changes across visual tasks: II. Decreases in cerebral cortex. *J. Cogn. Neurosci.* **9**, 648–663 (1997).
3. M. E. Raichle *et al.*, A default mode of brain function. *Proc. Natl. Acad. Sci. U.S.A.* **98**, 676–682 (2001).
4. M. J. Brookes *et al.*, Investigating the electrophysiological basis of resting state networks using magnetoencephalography. *Proc. Natl. Acad. Sci. U.S.A.* **108**, 16783–16788 (2011).
5. R. Mukamel *et al.*, Coupling between neuronal firing, field potentials, and fMRI in human auditory cortex. *Science* **309**, 951–954 (2005).
6. Y. Nir *et al.*, Coupling between neuronal firing rate, gamma LFP, and BOLD fMRI is related to interneuronal correlations. *Curr. Biol.* **17**, 1275–1285 (2007).
7. C. J. Keller *et al.*, Neurophysiological investigation of spontaneous correlated and anticorrelated fluctuations of the BOLD signal. *J. Neurosci.* **33**, 6333–6342 (2013).
8. B. L. Foster, V. Rangarajan, W. R. Shirer, J. Parvizi, Intrinsic and task-dependent coupling of neuronal population activity in human parietal cortex. *Neuron* **86**, 578–590 (2015).
9. A. L. Daitch *et al.*, Mapping human temporal and parietal neuronal population activity and functional coupling during mathematical cognition. *Proc. Natl. Acad. Sci. U.S.A.* **113**, E7277–E7286 (2016).
10. A. Kucyi *et al.*, Intracranial electrophysiology reveals reproducible intrinsic functional connectivity within human brain networks. *J. Neurosci.* **38**, 4230–4242 (2018).
11. R. Matsumoto *et al.*, Functional connectivity in the human language system: A cortico-cortical evoked potential study. *Brain* **127**, 2316–2330 (2004).
12. J. Parvizi, S. Kastner, Promises and limitations of human intracranial electroencephalography. *Nat. Neurosci.* **21**, 474–483 (2018).
13. C. J. Keller *et al.*, Mapping human brain networks with cortico-cortical evoked potentials. *Philos. Trans. R. Soc. Lond. B Biol. Sci.* **369**, 20130528 (2014).
14. C. J. Keller *et al.*, Intrinsic functional architecture predicts electrically evoked responses in the human brain. *Proc. Natl. Acad. Sci. U.S.A.* **108**, 10308–10313 (2011).
15. R. Matsumoto, T. Kunieda, D. Nair, Single pulse electrical stimulation to probe functional and pathological connectivity in epilepsy. *Seizure* **44**, 27–36 (2017).
16. J. M. Shine *et al.*, Distinct patterns of temporal and directional connectivity among intrinsic networks in the human brain. *J. Neurosci.* **37**, 9667–9674 (2017).
17. M. Esterman, S. K. Noonan, M. Rosenberg, J. Degutis, In the zone or zoning out? Tracking behavioral and neural fluctuations during sustained attention. *Cereb. Cortex* **23**, 2712–2723 (2013).
18. A. Kucyi *et al.*, Electrophysiological dynamics of antagonistic brain networks reflect attentional fluctuations. *Nat. Commun.* **11**, 325 (2020).
19. A. Kucyi, M. Esterman, C. S. Riley, E. M. Valera, Spontaneous default network activity reflects behavioral variability independent of mind-wandering. *Proc. Natl. Acad. Sci. U.S.A.* **113**, 13899–13904 (2016).
20. A. Kucyi, J. Parvizi, Pupillary dynamics link spontaneous and task-evoked activations recorded directly from human insula. *J. Neurosci.* **40**, 6207–6218 (2020).
21. B. H. Silverstein *et al.*, Dynamic tractography: Integrating cortico-cortical evoked potentials and diffusion imaging. *Neuroimage* **215**, 116763 (2020).
22. C. J. Honey *et al.*, Predicting human resting-state functional connectivity from structural connectivity. *Proc. Natl. Acad. Sci. U.S.A.* **106**, 2035–2040 (2009).
23. B. T. T. Yeo *et al.*, The organization of the human cerebral cortex estimated by intrinsic functional connectivity. *J. Neurophysiol.* **106**, 1125–1165 (2011).
24. O. Raccah, A. L. Daitch, A. Kucyi, J. Parvizi, Direct cortical recordings suggest temporal order of task-evoked responses in human dorsal attention and default networks. *J. Neurosci.* **38**, 10305–10313 (2018).
25. B. Fischl, M. I. Sereno, A. M. Dale, Cortical surface-based analysis. II: Inflation, flattening, and a surface-based coordinate system. *Neuroimage* **9**, 195–207 (1999).
26. Z. H. Guo *et al.*, Epileptogenic network of focal epilepsies mapped with cortico-cortical evoked potentials. *Clin. Neurophysiol.* **131**, 2657–2666 (2020).
27. D. M. Groppe *et al.*, iELVis: An open source MATLAB toolbox for localizing and visualizing human intracranial electrode data. *J. Neurosci. Methods* **281**, 40–48 (2017).
28. X. Papademetris *et al.*, BioImage Suite: An integrated medical image analysis suite: An update. *Insight J.* **2006**, 209 (2006).
29. J. R. Andrews-Hanna, J. S. Reidler, C. Huang, R. L. Buckner, Evidence for the default network's role in spontaneous cognition. *J. Neurophysiol.* **104**, 322–335 (2010).
30. E. Maris, R. Oostenveld, Nonparametric statistical testing of EEG- and MEG-data. *J. Neurosci. Methods* **164**, 177–190 (2007).